Biosensors and Bioelectronics 70 (2015) 89–97

Contents lists available at ScienceDirect

Biosensors and Bioelectronics

journal homepage: www.elsevier.com/locate/bios

A signal-on electrochemiluminescence biosensor for detecting Con A using phenoxy dextran-graphite-like carbon nitride as signal probe

Xin Ou [a], Xingrong Tan [b], Xiaofang Liu [a], Qiyi Lu [a], Shihong Chen [a,*], Shaping Wei [a,*]

[a] Key Laboratory of Luminescence and Real-Time Analytical Chemistry (Southwest University), Ministry of Education, College of Chemistry and Chemical Engineering, Southwest University, Chongqing 400715, People's Republic of China
[b] Department of Endocrinology, 9th People's Hospital of Chongqing, Chongqing 400700, People's Republic of China

ARTICLE INFO

Article history:
Received 29 November 2014
Received in revised form
22 February 2015
Accepted 9 March 2015
Available online 11 March 2015

Keywords:
Concanavalin A
Electrochemiluminescence biosensor
Graphite-like carbon nitride
Three-dimensional graphene
Gold nanoparticles

ABSTRACT

A novel signal-on electrochemiluminescence (ECL) biosensor for detecting concanavalin A (Con A) was fabricated with phenoxy dextran-graphite-like carbon nitride (DexP-g-C_3N_4) as signal probe. In this construction strategy, the nanocomposites of three-dimensional graphene and gold nanoparticles (3D-GR-AuNPs) were used as matrix for high loading of glucose oxidase (GOx), which served as recognition element for bounding Con A. Con A further interacted with DexP-g-C_3N_4 through a specific carbohydrate-Con A interaction to achieve a sandwiched scheme. With the increase of Con A incubated onto the electrode, the ECL signal resulted from DexP-g-C_3N_4 would enhance, thus achieving a signal-on ECL biosensor for Con A detection. Due to the integration of the virtues of 3D-GR-AuNPs and the excellent ECL performance of DexP-g-C_3N_4, the prepared biosensor exhibits a wide linear response range from 0.05 ng/mL to 100 ng/mL and a low detection limit of 17 pg/mL (S/N=3).

1. Introduction

Concanavalin A (Con A), a member of lectins family, is a carbohydrate-binding protein from jack bean with four saccharide binding sites (Tang et al., 2013; Chen et al., 2013a). Con A can exist in a form of dimer below pH 5.5 and a form of tetramer at neutral pH (Cella et al., 2010). Under neutral conditions, each subunit of Con A contains one site for hydrophobic recognition, one for calcium and manganese cation, which can activate the specificity carbohydrate site of protein, the third one for the specificity carbohydrate site for D-glucose or D-mannose residues (Hu et al., 2012; Liu et al., 2007). Con A can help the mature T cells to activate and proliferate. Meanwhile, the interaction between Con A and carbohydrate plays a crucial role in drug development and clinical diagnostics, such as the detection of leukemia cell and cancer cell (Pongracz et al., 2003; Zhang et al., 2013a; Hu and Zuo, 2013). Therefore, it is urgent to quantitate the Con A conveniently and rapidly. Up to now, various strategies and methods have been implemented to detect Con A, such as fluorescence technique (Zou et al., 2008), UV–vis spectrophotometry (Guo et al., 2007), and electrochemical method (Loaiza et al., 2011). Among these methods, electrochemiluminescence (ECL) biosensor is very attractive because of its high sensitivity, low background signal, well reproducibility, easy controllability, and wide dynamic response range (Jiang et al., 2014; Liu et al., 2015; Zhu et al., 2010, 2012). Moreover, the reports concerning ECL biosensor for detecting Con A is scarce now.

Since the first report on the cathodic electrochemiluminescence behavior of graphite-like carbon nitride (g-C_3N_4), g-C_3N_4 has been a new kind of promising luminophore candidate for ECL system and attracted much attention for its special structure and properties (Cheng et al., 2012, 2013a). $Ru(bpy)_3^{2+}$, a traditional luminophores, could be effected by many micro-environmental factors, such as temperature, ion strength (Dai et al., 2009). Compared with it, g-C_3N_4 presents many charming advantages, such as nontoxic, low cost, excellent biocompatibility (Chen et al., 2013b; Tian et al., 2013a). Furthermore, with the π-conjugated graphitic planes formed by the sp^2 hybridization of nitrogen and carbon, g-C_3N_4 has the smallest direct band gap (2.7 eV) and exhibits high thermal and chemical stability (Thomas et al., 2008; Zhou et al., 2013). More importantly, g-C_3N_4 can be easily manipulated post-functionalization or elementally doped. For instance, carbon nanotubes (Ge and Han, 2012), polyaniline (Lu et al., 2014b), Au (Cheng et al., 2013b) and Fe_3O_4 (Zhou et al., 2013) have been used to functionalize g-C_3N_4 to improve the properties of g-C_3N_4 and widen its application. Compared with the bulk g-C_3N_4, the ultrathin g-C_3N_4 nanosheet not only has better solubility, but also exhibits superior physiochemical properties such as larger surface area, thus has been applied into many works

* Corresponding authors. Fax: +86 23 68253172.
E-mail addresses: cshong@swu.edu.cn (S. Chen), shapingw@swu.edu.cn (S. Wei).

http://dx.doi.org/10.1016/j.bios.2015.03.021
0956-5663/

(Tian et al., 2013b; Cheng et al., 2013b). However, most reported sensors based on bulk g-C_3N_4 or g-C_3N_4 nanosheet were ECL signal-off type. For example, Chen et al. (2014) reported a signal-off ECL immunosensor for carcinoembryonic antigen based on a fact that carcinoembryonic antigen hindered the electron transfer, thus reduced the ECL intensity of AuNP-functionalized g-C_3N_4. For signal-off assays, there are challenges on the improvement of the assay sensitivity. Therefore, in the construction of ECL sensing system, signal-on assays with a high sensitivity is preferable.

Graphene, emerging as a two-dimensional monolayer of sp^2-hybridized carbon atoms, has aroused numerous interests for its exceptional physical and chemical properties, such as its good biocompatibility, fast electron transportation, good chemical and environmental stability (Huang et al., 2012; Geim, 2009; Chen et al., 2008). Especially, lots of works have been reported based on the two-dimensional graphene sheet in recent years (Bai et al., 2014; Yuan et al., 2013; Gui et al., 2014). Compared with two-dimensional graphene, three-dimensional graphene (3D-GR) exhibited outstanding characteristics, for example, high porosity and ultrahigh surface-to-volume ratio (Zhao et al., 2012; Xu et al., 2010), which offers great convenience to assemble more gold nanoparticles (AuNPs) on its surface for further improving the immobilization amount of biomolecules. More importantly, AuNPs could improve and stabilize the cathodic ECL intensity of g-C_3N_4 (Chen et al., 2014; Ou et al., 2014). Thus, the integration of 3D-GR and AuNPs would exhibit promising application prospect in the ECL biosensor.

Based on above observation, a signal-on ECL biosensor was developed with phenoxy dextran-graphite-like carbon nitride (DexP-g-C_3N_4) as signal probe to detect Con A. In this work, three-dimensional graphene-AuNPs (3D-GR-AuNPs) nanocomposites were synthesized via a hydrothermal reduction method without any extra reductants and used as matrix for high loading of glucose oxidase (GOx). The DexP-g-C_3N_4 as the signal probe was bound to the binding sites of Con A through a specific carbohydrate-Con A interaction (Huang et al., 2013a). During the fabrication of the electrode, GOx, Con A and DexP-g-C_3N_4 formed a sandwiched structure. With the increase of Con A incubated onto the electrode, the amount of DexP-g-C_3N_4 bound onto the modified electrode via the Con A would increase, thus resulting an enhancement of ECL signal, which was the quantitative foundation for the Con A detection. The details of the preparation, characterization, optimization of conditions and the response performances of the biosensor are followings.

2. Experimental

2.1. Reagents and chemicals

Melamine (2,4,6-triamino-1,3,5-trazine, 95%) was acquired from Aladdin Ltd. (Shanghai, China). Graphene oxide (GO) was obtained from Nanjing Xianfeng nano Co. (Nanjing, China). Concanavalin A (Con A) from canavalia ensiformis (jack bean), glucose oxidase (GOx, from Aspergillus niger), bovine serum albumin (BSA, 96%–99%), dextran (MW ≈ 70,000) and 1,2-epoxy-3-phenoxypropane (Epoxy) were all purchased from sigma (St. Louis, MO, USA). 0.10 M phosphate-buffered saline (PBS) solutions with various pH were produced with 0.10 M KH_2PO_4 and 0.10 M Na_2HPO_4. The supporting electrolyte was 0.10 M KCl. 0.10 M pH 7.0 PBS containing 0.10 mM $MnCl_2$ and 0.10 mM $CaCl_2$ were used to prepare Con A solution. Other chemicals used were of analytical grade and were used as received. Deionized water was used throughout the experiments.

2.2. Apparatus

Cyclic voltammetry (CV) and electrochemical impedance spectroscopy (EIS) experiments were performed using a CHI 600D electrochemical station (Shanghai CH Instruments Co., China). The ECL emission was conducted by a model MPI-A electrochemiluminescence analyzer (Xi'an Remax Electronic Science & Technology Co. Ltd., China). The spectral response range of the photomultiplier tube (PMT) was from 100 to 1000 V and the ECL emission wavelength was from 300 to 650 nm. The amplifying rate is three. The voltage of PMT was set at 600 V throughout the detection. A conventional three-electrode system was employed during the experiment with a saturated calomel electrode (SCE) or Ag/AgCl (sat. KCl) as reference electrode, a platinum wire as counter electrode and a modified glassy carbon electrode (GCE) as working electrode. The UV–visible (UV–vis) spectrometry was performed on a Lambda 17 UV–vis spectrometer 8500 (PE Co., USA) with the range of 200–800 nm. Fourier transform spectroscopy (FT-IR) was conducted on a Nexus 670 FT-IR spectrophotometer (Nicolet Instruments) with KBr as pellets. The morphology of nanocomposites was analyzed by a scanning electron microscopy (SEM, S-4800, Hitachi, Japan) and a transmission electron microscopy (TEM, JEM-1200EX). X-ray photoelectron spectroscopy (XPS) was test on Thermo ESCALAB 250 spectrometer (SID-Molecular).

2.3. Preparation of 3D-GR-AuNPs and DexP-g-C_3N_4 nanocomposites

3D-GR was prepared by a facile one-step hydrothermal method according to the literature with minor modification (Xu et al., 2010). 3D-GR-AuNPs nanocomposites were synthesized through a hydrothermal reduction without any extra reductants. The details of preparation of 3D-GR and 3D-GR-AuNPs were depicted in the supplementary materials.

The fabrication procedure of ultrathin g-C_3N_4 nanosheets was similar to the methods depicted by Tian et al. (2013b). Phenoxy dextran (DexP) was prepared according to the literature (Barone and Strano, 2006). DexP-g-C_3N_4 nanocomposites were fabricated via π–π stacking between g-C_3N_4 and DexP (Tang et al., 2013; Huang et al., 2013a). The details of preparation of g-C_3N_4 nanosheets and DexP-g-C_3N_4 were presented in the supplementary materials.

2.4. Fabrication of the biosensor

The glassy carbon electrode (GCE, Φ=4 mm) was polished with 0.3 μm and 0.05 μm alumina slurry, respectively, followed by ultrasonic rinse in ethanol and water. Then the electrode was allowed to dry in the air.

3D-GR-AuNPs suspension (15 μL) was dropped onto the surface of cleaned GCE. After 3D-GR-AuNPs modified electrode was air-dried at room temperature, 10 μL GOx (5 mg/mL) was casted on the surface for 10 h at 4 °C. Unbound GOx was removed by rinsing with PBS solution. Subsequently, 15 μL 0.2 wt% bovine serum albumin (BSA) was placed onto the electrode for 30 min to block non-specific adsorption. The resultant biosensor (BSA/GOx/3D-GR-AuNPs/GCE) was stored at 4 °C until further use. The fabricated procedure is schematically shown in Scheme 1.

2.5. The detection of Con A

The biosensor (BSA/GOx/3D-GR-AuNPs/GCE) was incubated with 15 μL Con A with different concentration for 30 min to achieve the assembly of Con A through specific binding between Con A and GOx (Kobayashi and Anzai, 2001). Then 15 μL DexP-g-C_3N_4 was further incubated on the modified electrode

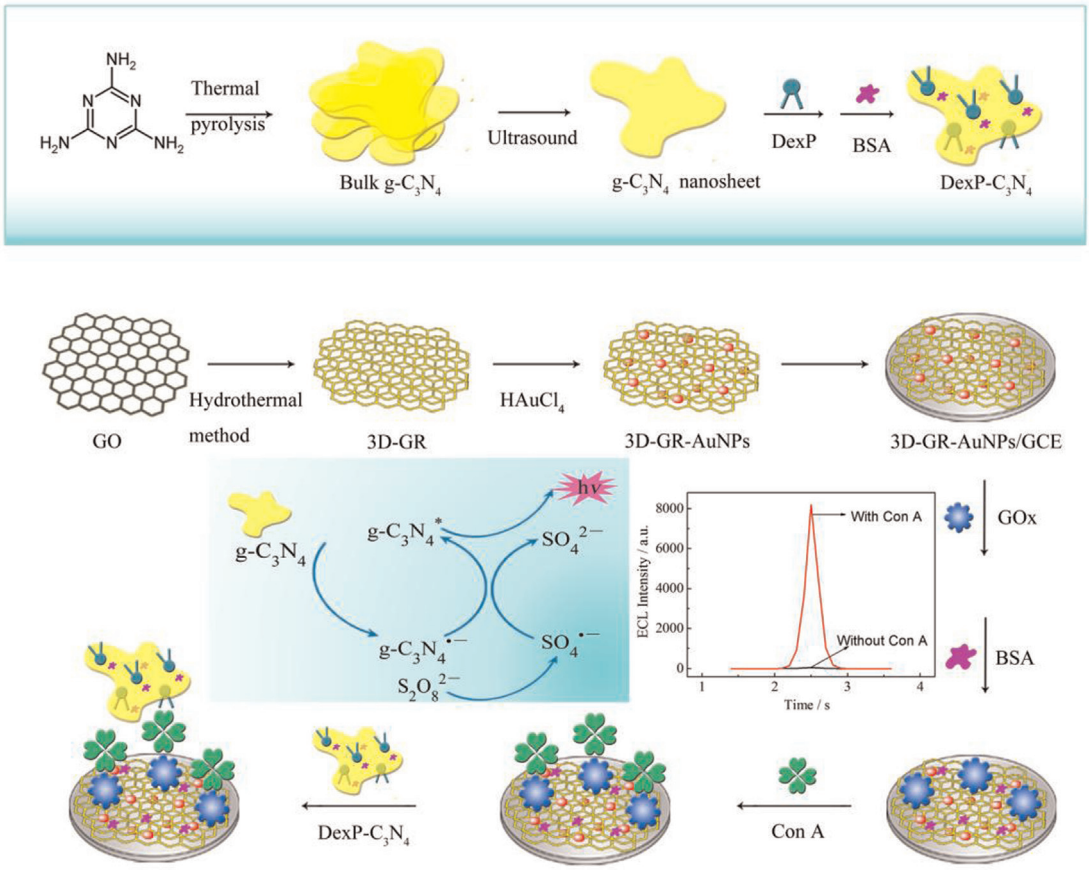

Scheme 1. The illustration of the synthetic process of DexP-g-C_3N_4 and 3D-GR-AuNPs and the preparation of the ECL biosensor.

surface for 30 min. In this step, DexP-g-C_3N_4 could be bound to the free binding sites of Con A to achieve a sandwich configuration. Finally, the obtained electrode was tested with an MPT-A ECL analyzer in 3 mL of 0.10 M PBS (pH 7.0) containing 0.10 M $K_2S_2O_8$. The resultant electrode was rinsed with PBS solution at every step. All measurements were operated at room temperature unless otherwise specified.

3. Results and discussion

3.1. Characterization of different nanomaterials

SEM and TEM were performed to characterize the microstructure and morphology of as-prepared nanomaterials. As seen in the SEM and TEM images of GO, typically crumpled and wrinkled structure, as well as the monolayer structure, could be clearly observed (Fig. 1A and B). Fig. 1C and D present the SEM and TEM images of 3D-GR, respectively. As expected, both SEM and TEM images displayed the interconnected 3D porous networks, which were obviously different from the images of GO, indicating the successful preparation of 3D-GR. When AuNPs were in situ generated on the 3D-GR, the SEM image (Fig. 1E) and TEM image (Fig. 1F) clearly showed the presence of numerous gold nanoparticles on the interconnected 3D porous networks, demonstrating that the 3D-GR-AuNPs were successful synthesized. For the g-C_3N_4 nanosheets, the TEM image clearly displayed the nanosheets structure (Fig. 1G), indicating that g-C_3N_4 nanosheets were exfoliated from bulk g-C_3N_4.

The UV–vis absorption spectroscopy was conducted to investigate the 3D-GR-AuNPs and DexP-g-C_3N_4. As shown in Fig. 2A curve a, a strong absorption peak at 258 nm was detected in 3D-GR, ascribing to the characteristic peak of graphene (Dong et al., 2015). When AuNPs were conjugated on the 3D-GR (Fig. 2A curve b), a new absorption peak appeared at 529 nm, which was assigned to the surface plasma resonance absorption band of gold nanoparticles (Huang et al., 2013a). In the UV–vis absorption spectrum of the g-C_3N_4 nanosheets (Fig. 2B curve a), an absorption peak at 324 nm was obviously observed, ascribing to the characteristic peak of g-C_3N_4 (Tian et al., 2013b). For the as-prepared DexP, two remarkable absorption peaks at 218 nm and 270 nm were observed (Fig. 2B curve b), demonstrating that the dextran derivative DexP had been successfully prepared (Huang et al., 2013b). After DexP was stacked onto g-C_3N_4, the characteristic peaks of DexP red-shifted to 220 nm and 277 nm in the DexP-g-C_3N_4 (Fig. 2B curve c), respectively. Above results indicate the successful stack of DexP on g-C_3N_4. Moreover, FT-IR absorption spectrum analysis also provided effective information for the immobilization of DexP on g-C_3N_4. For the g-C_3N_4 nanosheet (Fig. 2C curve a), the characteristic broad peak between 3000 and 3600 cm^{-1} was assigned to the N–H stretching. The bands between 1000 and 1800 cm^{-1} were contributed to the stretching vibration of connected units of C–NH–C (partial condensation) or C–N(–C)–C (full condensation). The sharp peak at around 811 cm^{-1} was corresponded to the heptazine ring system (Zhang et al., 2013b). In the spectrum of DexP (Fig. 2C curve b), two absorption peaks at 917 cm^{-1} and 1153 cm^{-1} were observed, assigning to the characteristic peaks of epoxy group and phenoxy group (Huang et al., 2013b). When DexP was stacked onto g-C_3N_4, DexP-g-C_3N_4 presented all characteristic peaks of both DexP and g-C_3N_4 (Fig. 2C curve c), indicating the successful synthesis of DexP-g-C_3N_4 via π–π stacking between g-C_3N_4 and DexP.

To further gain the information concerning the chemical composition of g-C_3N_4 and DexP-g-C_3N_4, XPS measurements were

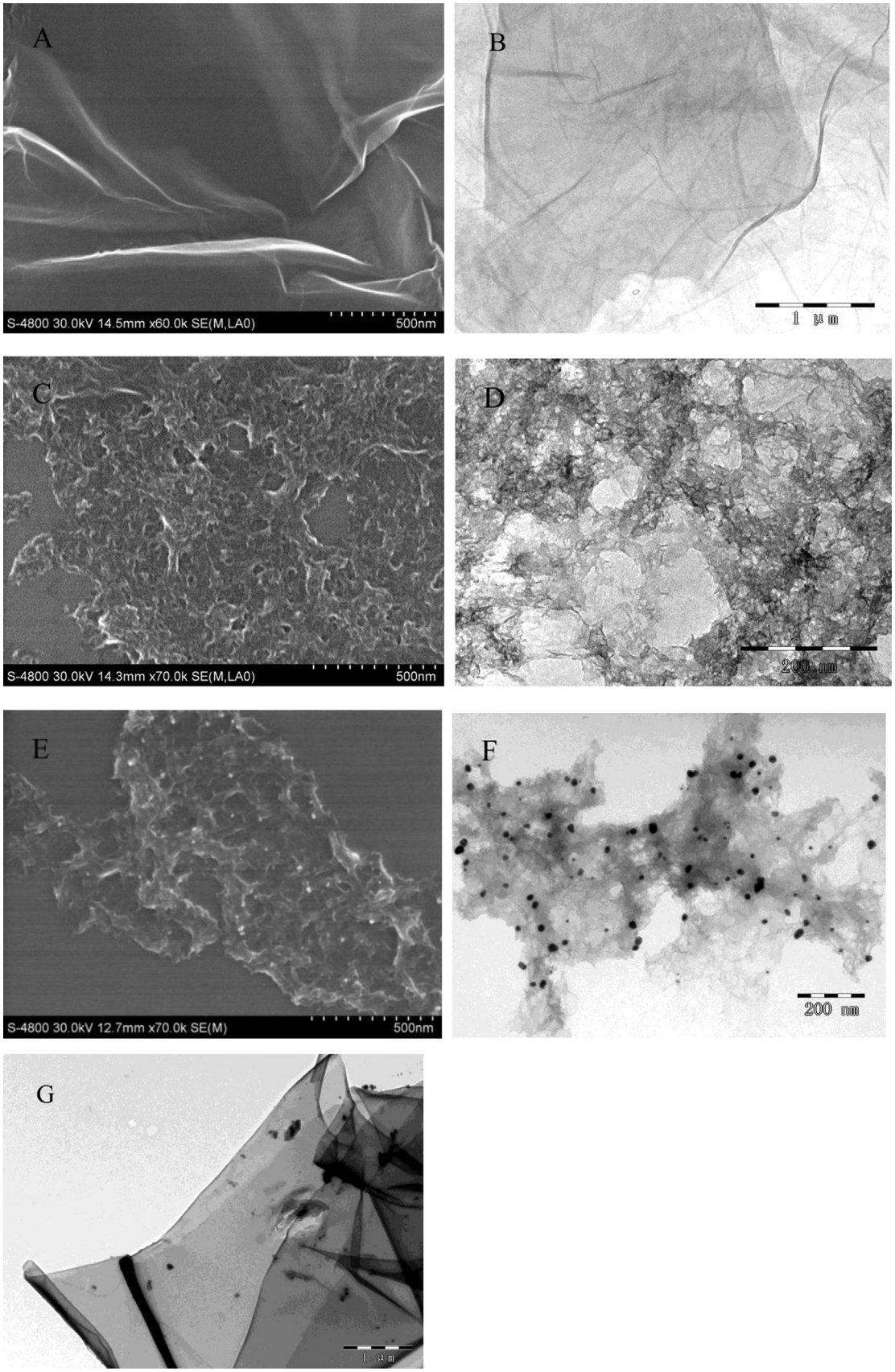

Fig. 1. SEM images of (A) GO, (C) 3D-GR, (E) 3D-GR-AuNPs. TEM images of (B) GO, (D) 3D-GR, (F) 3D-GR-AuNPs and (G) g-C_3N_4 nanosheet.

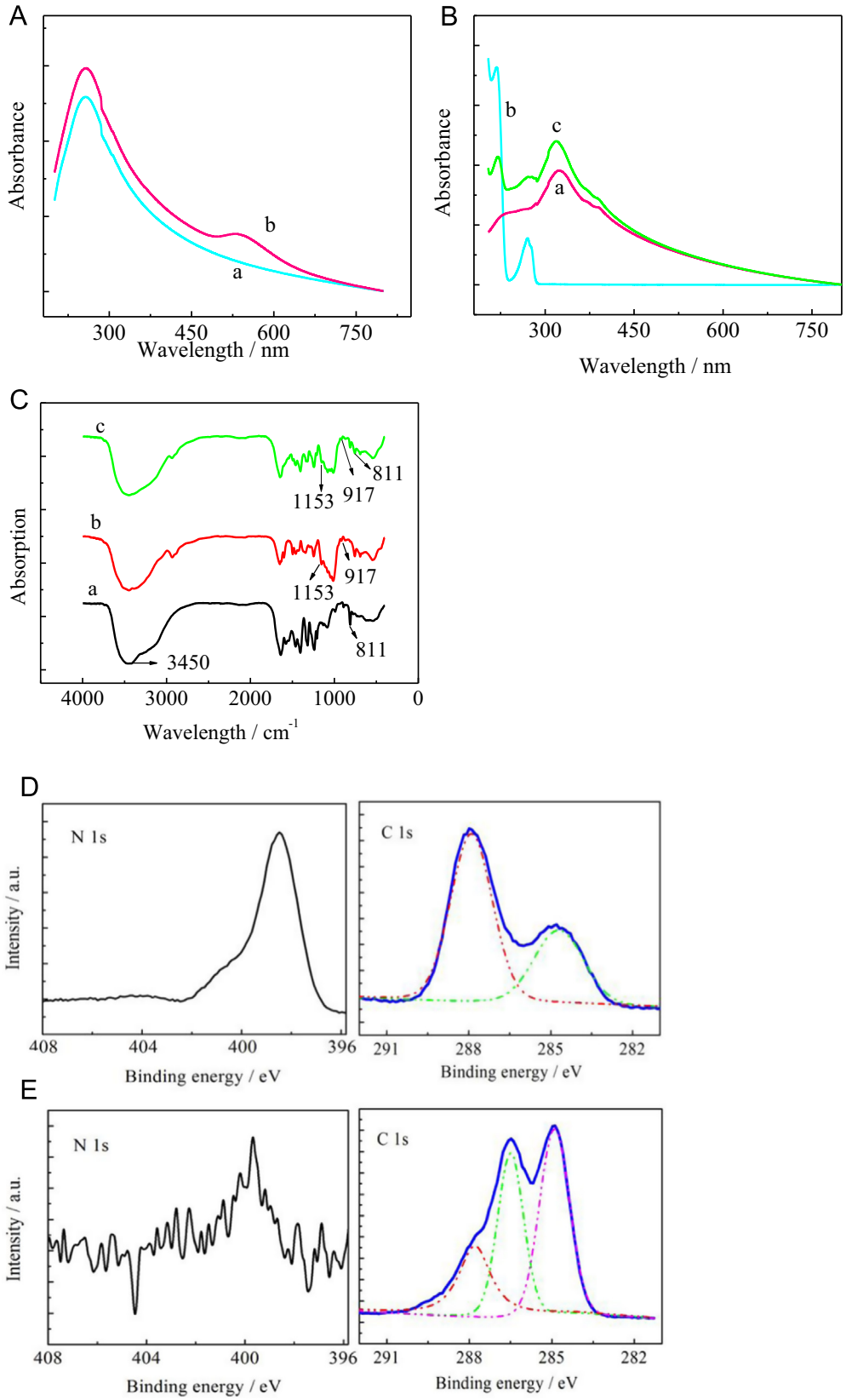

Fig. 2. (A) UV–vis absorption spectra of (a) 3D-GR and (b) 3D-GR-AuNPs; (B) UV–vis and (C) FT-IR absorption spectra of (a) g-C_3N_4, (b) DexP and (c) DexP-g-C_3N_4; The XPS spectra of (D) g-C_3N_4 and (E) Dexp-g-C_3N_4.

performed and the results are shown in Fig. 2D and E, respectively. The N 1s peak was observed in both Fig. 2D and E, which was ascribed to the N of the g-C_3N_4 nanosheets. Furthermore, the N content decreased from 37 to 1% when g-C_3N_4 nanosheets were conjugated with DexP. This is may be due to the fact that the DexP only contains C and O, and without N. The C 1s peak of g-C_3N_4

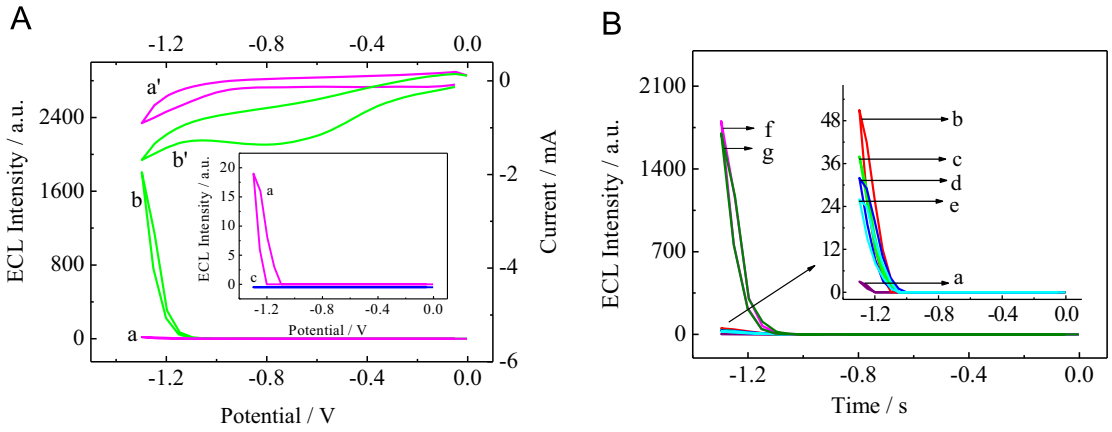

Fig. 3. (A) ECL (a, b) and CV (a', b') curves of DexP-g-C_3N_4/Con A/BSA/GOx/3D-GR-AuNPs/GCE in PBS (pH 7.0) without (a, a') and with (b, b') 0.10 M $K_2S_2O_8$. Inset: ECL profiles of (a) DexP-g-C_3N_4/Con A/BSA/GOx/3D-GR-AuNPs/GCE and (c) Con A/BSA/GOx/3D-GR-AuNPs/GCE in PBS (pH 7.0) without 0.10 M $K_2S_2O_8$. (B) ECL behaviors of (a) bare GCE, (b) 3D-GR-AuNPs/GCE, (c) GOx/3D-GR-AuNPs /GCE, (d) BSA/GOx/3D-GR-AuNPs/GCE, (e) Con A/BSA/GOx/3D-GR-AuNPs/GCE and (f) DexP-g-C_3N_4/Con A/BSA/GOx/3D-GR-AuNPs/GCE in PBS (pH 7.0) containing 0.10 M $K_2S_2O_8$, (g) DexP-g-C_3N_4/Con A/BSA/GOx/3D-GR-AuNPs/GCE in N_2-saturated PBS (pH 7.0) containing 0.10 M $K_2S_2O_8$.

could be fitted by two components with the binding energy 287.9 eV and 284.7 eV (Fig. 2D), respectively, which were assigned to the sp^2-bonded C atoms of g-C_3N_4 and the C atoms in a pure carbon environment. However, the C 1s peak of DexP-g-C_3N_4 could be fitted by three components (Fig. 2E). Besides the sp^2-bonded C atoms with the binding energy 287.9 eV and the carbon atoms in a pure carbon environment with the binding energy 284.7 eV, another component was observed at 286.4 eV, which was attributable to the C–O specie in DexP. Above results well confirmed the formation of DexP-g-C_3N_4.

3.2. ECL and CV behaviors of the modified electrodes

ECL and CV behaviors of the modified electrodes were investigated. The insert of Fig. 3A presents the ECL profiles of DexP-g-C_3N_4/Con A/BSA/GOx/3D-GR-AuNPs/GCE (curve a) and Con A/BSA/GOx/3D-GR-AuNPs/ GCE (curve c) in the absence of $K_2S_2O_8$. As seen, no ECL signal was observed at curve c, and a very weak ECL signal appeared at curve a, which was due to the weak ECL reaction between g-C_3N_4 and dissolved oxygen (Eq. 1 to Eq. 4) (Chen et al., 2014, 2013b). Here, g-C_3N_4 was a luminophore. In order to investigate the role of $K_2S_2O_8$, the ECL behaviors were compared at DexP-g-C_3N_4/Con A/BSA/GOx/3D-GR-AuNPs/GCE in absence and presence of 0.10 M $K_2S_2O_8$, and the results are shown in curve a and curve b, respectively. As observed, the modified electrode showed a greatly enhanced ECL signal in the presence of 0.10 M $K_2S_2O_8$ (curve b), confirming a fact that $K_2S_2O_8$ as coreactant could greatly improve the ECL intensity of g-C_3N_4. The corresponding CV curves of DexP-g-C_3N_4/Con A/BSA/GOx/3D-GR-AuNPs/GCE in the absence (curve a') and presence (curve b') of $K_2S_2O_8$ were also provided in the Fig. 3A. As depicted, when the scan potential was more negative than −0.90 V, the reduction currents increased sharply at the both curve a' and curve b', assigning to the electro-reduction of g-C_3N_4 (Cheng et al., 2012). Meanwhile, a broad cathodic wave with a shoulder peak at around −0.7 V was found at curve b' and no broad peak was observed for curve a', indicating a fact that the broad cathodic wave at curve b' was due to the electro-reduction of coreactant $S_2O_8^{2-}$. The possible mechanism of ECL response was proposed (Cheng et al., 2012). Firstly, g-C_3N_4 was reduced to g-$C_3N_4^{\bullet-}$ (Eq. 1). Meanwhile, $S_2O_8^{2-}$ was reduced to $SO_4^{\bullet-}$ (Eq. 5). Subsequently, $SO_4^{\bullet-}$ could react with g-$C_3N_4^{\bullet-}$ to produce the excited state g-C_3N_4* (Eq. 6), giving the ECL emission (Eq. 9). Another possible way to generate g-C_3N_4* can be described by (Eqs. (4) and 5). Since $SO_4^{\bullet-}$ is powerful oxidant, it may oxidize g-C_3N_4 to g-$C_3N_4^{+}$ (Eq. 7). g-$C_3N_4^{+}$ further reacted with g-$C_3N_4^{\bullet-}$ to produce g-C_3N_4*, then generating ECL emission (Eq. 8 and Eq. 9). The mechanism was described as follows.

$$g\text{-}C_3N_4 + e^- \rightarrow g\text{-}C_3N_4^{\bullet-} \quad (1)$$

$$O_2 + 2H_2O + 2e \rightarrow 2H_2O_2 \quad (2)$$

$$2H_2O_2 + e \rightarrow OH^- + OH^{\bullet} \quad (3)$$

$$g\text{-}C_3N_4^{\bullet-} + OH^{\bullet} \rightarrow g\text{-}C_3N_4^{*} + OH^- \quad (4)$$

$$S_2O_8^{2-} + e^- \rightarrow SO_4^{2-} + SO_4^{\bullet-} \quad (5)$$

$$g\text{-}C_3N_4^{\bullet-} + SO_4^{\bullet-} \rightarrow g\text{-}C_3N_4^{*} + SO_4^{2-} \quad (6)$$

and / or

$$g\text{-}C_3N_4 + SO_4^{\bullet-} \rightarrow g\text{-}C_3N_4^{+} + SO_4^{2-} \quad (7)$$

$$g\text{-}C_3N_4^{+} + g\text{-}C_3N_4^{\bullet-} \rightarrow g\text{-}C_3N_4^{*} + g\text{-}C_3N_4 \quad (8)$$

Finally,

$$g\text{-}C_3N_4^{*} \rightarrow C_3N_4 + h\nu \quad (9)$$

3.3. ECL, CV and EIS characterization of stepwise fabrication of the electrode

The stepwise fabrication of the electrode was characterized by ECL in PBS (pH 7.0) containing 0.10 M $K_2S_2O_8$. As depicted in the Fig. 3B, a quite weak ECL intensity appeared at bare electrode (curve a). This was due to the fact that $OOH^{\bullet}$ produced by dissolved O_2 reacted with $SO_4^{\bullet-}$ to obtain $(O_2)_2$*, which acted as light-emitting species to generate ECL emission (Lu et al., 2014a; Yao et al., 2008). This phenomenon was previously reported by Li et al. (2015). After 3D-GR-AuNPs were modified onto the GCE (curve b), an enhanced ECL intensity was observed because of the fast electron transportation of 3D-GR-AuNPs. But the intensity was still weak. When GOx, BSA and Con A were successively modified onto the electrode (curves c–e), continuous decreased ECL intensity was observed because of the obstacle of these non-conductive materials. However, with the incubation of DexP-g-C_3N_4 (curve f), the obtained sensor presented a greatly enhanced ECL signal, which resulted from the reaction of luminophore (g-C_3N_4) and coreactant ($S_2O_8^{2-}$). To exclude the effect of dissolved O_2, the biosensor was also tested in N_2-saturated PBS (pH 7.0) containing 0.10 M $K_2S_2O_8$ (curve g). No obvious change in ECL intensity was

observed, indicating that the effect of dissolved O_2 on the ECL behavior of g-C_3N_4 was nearly ignored (Chen et al., 2014; Cheng et al., 2012).

In order to further confirm the fabrication process of the modified electrode, CV and EIS characterization was performed. The results were exhibited in Fig. S1A and S1B, respectively, demonstrating the successful fabrication of the electrode. The corresponding expression of the stepwise assembly of the electrode was shown in supplementary materials.

3.4. Optimization of experimental conditions

To obtain the excellent performance of the prepared ECL biosensor for Con A detection, the $K_2S_2O_8$ concentration, pH of the detection solutions and incubation time of Con A, were optimized. The corresponding depictions were presented in supplementary materials.

3.5. Performance of the biosensor

Under the optimized experimental conditions, the performance of the proposed biosensor was explored by incubating the standard Con A solution with different concentrations. As depicted in Fig. 4A, the ECL signal increased gradually with increasing the concentration of Con A and the corresponding calibration curve for Con A detection is shown in Fig. 4B. A good linear relationship was found between the ECL intensity and the concentration of Con A from 0.05 ng/mL to 100 ng/mL. The regression equation was I (a.u.) $=278.2+159.9\ C$ (ng/mL) ($R^2=0.9970$) and the detection limit was 17 pg/mL (S/N=3). When the Con A concentration was more than 100 ng/mL, the plateau effect was reached since only a slight increase in the ECL intensity was observed with further increasing the concentration of Con A. Compared with other methods of Con A detection (Table 1), the biosensor in this work performed a lower detection limit down to 10^{-5} μg/mL. Furthermore, our prepared biosensor also exhibited a high sensitivity and wide dynamic response range, achieving four orders of magnitude. This may be due to the following facts. On the one hand, g-C_3N_4 oneself exhibited an excellent ECL behavior and can generate a strong ECL intensity in cathodic potentials. On the other hand, the introduction of 3D-GR and AuNPs with excellent biocompatibility and large surface area can immobilize more GOx on the electrode, leading to a higher loading of Con A and g-C_3N_4 on the electrode, thus resulting in an obvious improvement in strong ECL intensity. Moreover, the ECL technique has high sensitivity.

To verify the role of DexP-g-C_3N_4 nanocomposites, as control experiments, the ECL response of g-C_3N_4/Con A/BSA/GOx/3D-GR-AuNPs/GCE and DexP/Con A/BSA/GOx/3D-GR-AuNPs/GCE were investigated. As shown in Fig. 4C, a weak ECL intensity was obtained at the control electrode g-C_3N_4/Con A/BSA/GOx/3D-GR-AuNPs/GCE without DexP (curve a). This may be due to the fact that g-C_3N_4 can not be specifically bound with Con A in the absence of DexP. In addition, an analogical weak ECL intensity was also observed at DexP/BSA/GOx/3D-GR-AuNPs/GCE without luminescence reagent g-C_3N_4 (curve b). However, as expected, a strong ECL intensity was obtained at the electrode with both DexP and g-C_3N_4 (curve c). Obviously, in this work, the DexP-g-C_3N_4 not only served as an excellent ECL signal probe, but also played another important role, namely it could specifically bound with the Con A through a specific carbohydrate-Con A interaction, thus achieving a novel sandwich-type scheme with a signal-on ECL detection strategy.

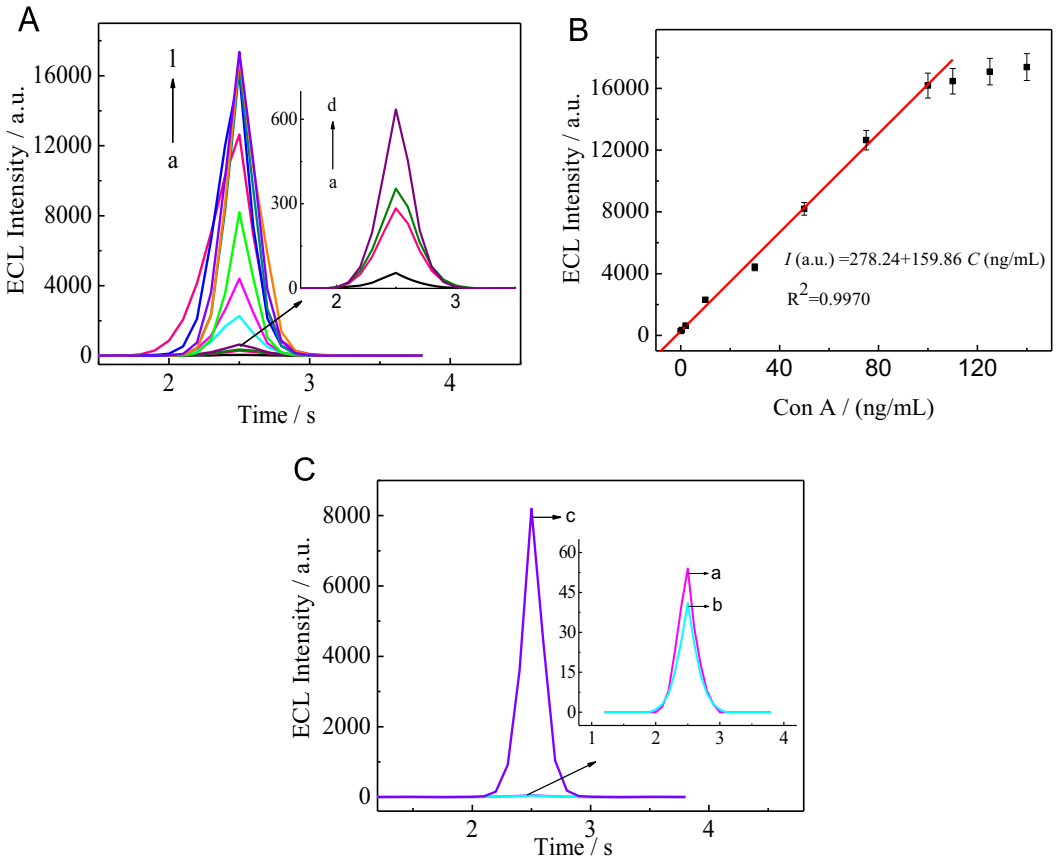

Fig. 4. (A) ECL response of the biosensor to (a) 0, (b) 0.05, (c) 0.5, (d) 2, (e) 10, (f) 30, (g) 50, (h) 75, (i) 100, (j) 110 (k) 125 (l) 140 ng/mL Con A in PBS (pH 7.0) containing 0.10 M $K_2S_2O_8$. (B) Calibration curve at different concentration of Con A (C) ECL intensity comparison of (a) g-C_3N_4/Con A/BSA/GOx/3D-GR-AuNPs/GCE, (b) DexP/Con A/BSA/GOx/3D-GR-AuNPs/GCE and (c) DexP-g-C_3N_4/Con A/BSA/GOx/3D-GR-AuNPs/GCE in PBS (pH 7.0) containing 0.10 M $K_2S_2O_8$.

Table 1
Comparison of different methods for the determination of Con A.

Method	Linear range (μg/mL)	Detection limit (μg/mL)	Reference
Surface plasmon resonance	1.0–20.0	0.39	Huang et al., (2013a)
Electrochemistry	3.4×10^{-4}–9.5×10^{-1}	1.1×10^{-4}	Hu et al., (2012)
Fluorescence	10.2–255	7.7	Huang et al., (2009)
Quartz crystal monitor	51–459	–	Zeng et al., (2014)
Electrochemiluminescence	5.0×10^{-5}–1.0×10^{-1}	1.7×10^{-5}	This work

3.6. Stability, reproducibility and selectivity of the proposed biosensor

The stability of proposed biosensor was tested by successive scans at the same biosensor with 25 ng/mL Con A in working buffer. As depicted in Fig. S3A, the ECL intensity did't show obvious changes and the relative standard deviation (RSD) was 2.2% for 10 cycles. In addition, the long-term storage stability was investigated at 10 ng/mL Con A by storing the biosensor at 4 °C and testing every three days. The response of the biosensor maintained 91.5% of the initial response, after storing for 15 days. The reproducibility of biosensor was also measured by using five proposed biosensors incubated the same concentration of Con A (10 ng/mL) in the same condition. Five biosensors exhibited a similar ECL response and the RSD was 5.7%. These results indicated that the biosensor exhibited an acceptable stability and reproducibility.

To further investigate the specificity and selectivity of the prepared biosensor, interference experiments were accomplished. As pictured in Fig. S3B, the change in ECL response resulted from BSA, cytochrome c (Cyt C) and phytohemagglutinin (PHA) was negligible when compared to the case obtained in the blank solution. Meanwhile, when the biosensor was incubated with Con A containing BSA, Cyt C and PHA, there was no remarkable change of ECL intensity in comparison with the biosensor incubated with Con A only. Above results suggested an acceptable selectivity.

3.7. Application of the biosensor

To evaluate the potential application of the proposed biosensor in the detection of real samples, the recovery experiments of Con A were tested in human serum samples via a standard addition method. The four samples were diluted with PBS. The recoveries were in the range of 94.2–104%, demonstrating the practicability of our biosensor for Con A detection in real biological samples (Table S1).

4. Conclusion

In summary, a novel sandwich-type ECL biosensor for detecting Con A was successfully fabricated with DexP-g-C_3N_4 as signal probe. The main contribution in this work is concentrated on the preparation of a novel DexP-g-C_3N_4 hybrid and its application in the construction of signal-on sandwiched ECL biosensor. Such a signal-on based ECL biosensor exhibited a high sensitivity and low detection limit for the determination of Con A. The applied limitation of this biosensor lies in its relatively longer preparation time. The total assay time may be shorten through combining the GOx and 3D-GR-AuNPs nanocomposites in advance to avoid the long incubation time of GOx onto the electrode. The combination of 3D-GR-AuNPs and DexP-g-C_3N_4 would provide a promising approach to fabricate signal-on ECL sensing.

Acknowledgements

This work was supported by National Natural Science Foundation of China (21075100, 21275119), Ministry of Education of China (708073), Science and Technology Commission of Beibei (2012-27), Medical Scientific Research Projects of Health Bureau of Chongqing (2012-2-286), State Key Laboratory of Electroanalytical Chemistry (SKLEAC 2010009), Specialized Research Fund for the Doctoral Program of Higher Education (swu113029), Natural Science Foundation Project of Chongqing City (CSTC-2011BA7003, CSTC-2014JCYJA20005) and Fundamental Research Funds for the Central Universities (XDJK2012A004, XDJK2013C115).

Appendix A. Supplementary material

Supplementary data associated with this article can be found in the online version at http://dx.doi.org/10.1016/j.bios.2015.03.021.

References

Bai, L.J., Chai, Y.Q., Pu, X.Y., Yuan, R., 2014. Nanoscale 6, 2902–2908.
Barone, P.W., Strano, M.S., 2006. Angew. Chem. Int. Ed. 118, 8318–8321.
Cella, L.N., Chen, W., Myung, N.V., Mulchandani, A., 2010. J. Am. Chem. Soc. 132, 5024–5026.
Chen, H., Muller, M.B., Gilmore, K.J., Wallace, G.G., Li, D., 2008. Adv. Mater. 20, 3557–3561.
Chen, L.C., Huang, D.J., Ren, S.Y., Dong, T.Q., Chi, Y.W., Chen, G.N., 2013b. Nanoscale 5, 225–230.
Chen, L.C., Zeng, X.T., Si, P., Chen, Y.M., Chi, Y.W., Kim, D.H., Chen, G.N., 2014. Anal. Chem. 86, 4188–4195.
Chen, Z.H., Liu, Y., Wang, Y.Z., Zhao, X., Li, J.H., 2013a. Anal. Chem. 85, 4431–4438.
Cheng, C.M., Huang, Y., Tian, X.Q., Zheng, B.Z., Li, Y., Yuan, H.Y., Xiao, D., Xie, S.P., Choi, M.M.F., 2012. Anal. Chem. 84, 4754–4759.
Cheng, C.M., Huang, Y., Wang, Jun, Zheng, B.Z., Yuan, H.Y., Xiao, D., 2013a. Anal. Chem. 85, 2601–2605.
Cheng, N.Y., Tian, J.Q., Liu, Q., Ge, C.J., Qusti, A.H., Asiri, A.M., Al-Youbi, A.O., Sun, X.P., 2013b. Appl. Mater. Interfaces 5, 6815–6819.
Dai, H., Wang, Y.M., Wu, X.P., Zhang, L., Chen, G.N., 2009. Biosens. Bioelectron. 24, 1230–1234.
Dong, Y.P., Gao, T.T., Zhou, Y., Chu, X.F., Wang, C.M., 2015. Spectrochim. Acta Part A: Mol. Biomol. Spectrosc. 134, 225–232.
Geim, A.K., 2009. Science 324, 1530–1534.
Ge, L., Han, C.C., 2012. Appl. Catal. 117–118, 268–274.
Gui, G.F., Zhuo, Y., Chai, Y.Q., Xiang, Y., Yuan, R., 2014. Anal. Chem. 86, 5873–5880.
Guo, C.X., Boullanger, P., Jiang, L., Liu, T., 2007. Biosens. Bioelectron. 22, 1830–1834.
Hu, F.X., Chen, S.H., Wang, C.Y., Yuan, R., Xiang, Y., Wang, C., 2012. Biosens. Bioelectron. 34, 202–207.
Hu, Y.F., Zuo, P., Y., B.C., 2013. Biosens. Bioelectron. 43, 79–83.
Huang, C.F., Yao, G.H., Liang, R.P., Qiu, J.D., 2013a. Biosens. Bioelectron. 50, 305–310.
Huang, C.C., Chen, C.T., Shiang, Y.C., Lin, Z.H., Chang, H.T., 2009. Anal. Chem. 81, 875–882.
Huang, J., Zhang, L., Liang, R.P., Qiu, J.D., 2013b. Biosens. Bioelectron. 41, 430–435.
Huang, X., Qi, X., Boey, F., Zhang, H., 2012. Chem. Soc. Rev. 41, 666–686.
Jiang, X.Y., Chai, Y.Q., Wang, H.J., Yuan, R., 2014. Biosens. Bioelectron. 54, 20–26.
Kobayashi, Y., Anzai, J.I., 2001. J. Electroanal. Chem. 507, 250–255.
Li, X.J., Guo, Z.K., Li, J.X., Zhang, Y., Ma, H.M., Pang, X.H., Du, B., 2015. Anal. Chim. Acta. 854, 40–46.
Liu, L.L., Ma, Q., Yang, L., Liu, Z.P., Su, X.G., 2015. Biosens. Bioelectron. 63, 519–524.
Liu, S.Q., Wang, K.W., Du, D., Sun, Y.M., He, L., 2007. Biomacromolecules 8, 2142–2148.
Loaiza, O.A., Lamas-Ardisana, P.J., Jubete, E., Ochoteco, E., Loinaz, I., Cabanero, G., Garcia, I., Penades, S., 2011. Anal. Chem. 83, 2987–2995.
Lu, Q.Y., Hu, H.X., W., Y.Y., Chen, S.H., Yuan, D.H., Yuan, R., 2014a. Biosens.

Bioelectron. 60, 325–331.
Lu, Q.Y., Zhang, J.J., Liu, X.F., Wu, Y.Y., Yuan, R., Chen, S.H., 2014b. Analyst 139, 6556–6562.
Ou, X., Tan, X.R., W., S.P., Chen, S.H., Zhang, J.J., Liu, X.F., 2014. Anal. Methods 6, 3804–3810.
Pongracz, J., Parnell, S., Anderson, G., Jaffrezou, J.P., Jenkinson, E., 2003. Mol. Immunol. 39, 1013–1023.
Tang, D.P., Zhang, B., Tang, J., Li, H., Chen, G.N., 2013. Anal. Chem. 85, 6958–6966.
Thomas, A., Fischer, A., Goettmann, F., Antonietti, M., Muller, J.O., Schlogl, R., Carlsson, J.M., 2008. J. Mater. Chem. 18, 4893–4908.
Tian, J.Q., Liu, Q., Asiri, A.M., Al-Youbi, A.O., Sun, X.P., 2013b. Anal. Chem. 85, 5595–5599.
Tian, J.Q., Liu, Q., Ge, C.J., Xing, Z.C., Asiri, A.M., Al-Youbi, A.O., Sun, X.P., 2013a. Nanoscale 5, 8921–8924.
Xu, Y.X., Sheng, K.X., Li, C., Shi, G.Q., 2010. ACS Nano 4, 4324–4330.
Yao, W., Wang, L., Wang, H.Y., Zhang, X.L., 2008. Electrochim. Acta 54, 733–737.
Yuan, D.H., Chen, S.H., Yuan, R., Zhang, J.J., Zhang, W., 2013. Analyst 138, 6001–6006.
Zeng, H.J., Yu, J.S., Jiang, Y.D., Zeng, X.Q., 2014. Biosens. Bioelectron. 55, 157–161.
Zhang, M., Liu, H., Chen, L., Yan, M., Ge, L., Ge, S.G., Yu, J.H., 2013a. Biosens. Bioelectron. 49, 79–85.
Zhang, X.D., Xie, X., Wang, H., Zhang, J.J., Pan, B.C., Xie, Y., 2013b. J. AM. Chem. Soc 135, 18–21.
Zhao, Y., Hu, C.G., Hu, Y., Cheng, H.H., Shi, G.Q., Qu, L.T., 2012. Angew. Chem. Int. Ed. 51, 11371–11375.
Zhou, X.S., Jin, B., Chen, R.Q., Peng, F., Fang, Y.P., 2013. Mater. Res. Bull. 48, 1447–1452.
Zhu, D.B., Zhou, X.M., Xing, D., 2010. Biosens. Bioelectron. 26, 285–288.
Zhu, D.B., Zhou, X.M., Xing, D., 2012. Anal. Chim. Acta. 725, 39–43.
Zou, L., Pang, H.L., Chan, P.H., Huang, Z.S., Gu, L.Q., Wong, K.Y., 2008. Carbohyd. Res. 343, 2932–2938.